

PAPER

## Droplet-jet mode near-field electrospinning for controlled helix patterns with sub-10 $\mu\text{m}$ coiling diameter

To cite this article: Dongwoon Shin *et al* 2019 *J. Micromech. Microeng.* **29** 045004

View the [article online](#) for updates and enhancements.



**IOP | ebooks<sup>TM</sup>**

Bringing you innovative digital publishing with leading voices to create your essential collection of books in STEM research.

Start exploring the collection - download the first chapter of every title for free.

# Droplet-jet mode near-field electrospinning for controlled helix patterns with sub-10 $\mu\text{m}$ coiling diameter

Dongwoon Shin<sup>1</sup>, Jonghyun Kim<sup>1</sup>, Sun Choi<sup>2</sup>, Yong-bok Lee<sup>2</sup>  
and Jiyoung Chang<sup>1,3</sup>

<sup>1</sup> Department of Mechanical Engineering, University of Utah, Salt Lake City, UT 84112, United States of America

<sup>2</sup> Korea Institute of Science and Technology, Seoul, Republic of Korea

E-mail: [jy.chang@utah.edu](mailto:jy.chang@utah.edu)

Received 4 December 2018, revised 11 January 2019

Accepted for publication 28 January 2019


Published 21 February 2019



## Abstract

This study presents a novel droplet-jet mode of near-field electrospinning which allows microscale control of helix patterns using nanofiber. While the cone-jet mode has been used to generate a printable nanofiber to date, the cone-jet mode requires a high applied voltage with a long jet travel distance to obtain the nanofiber, resulting in a large coiling diameter. In order to integrate the near-field electrospinning into microscale devices, it is important to achieve a comparable nanofiber pattern resolution. Herein, we have demonstrated printing of nanofibers with a coiling diameter of sub-10  $\mu\text{m}$ , which is produced by the droplet-jet mode of near-field electrospinning. Also, it is found that the coiling diameter, wavelength, and frequency can be controlled by the droplet size as one of the process parameters in the droplet-jet mode. The droplet-jet mode will be a promising near-field electrospinning technique to apply direct-written nanofibers to various micro-scale applications.

Keywords: nanofiber, near-field electrospinning, droplet, electrohydrodynamic printing, microscale printing, direct-writing

 Supplementary material for this article is available [online](#)

(Some figures may appear in colour only in the online journal)

## 1. Introduction

Nanofiber has garnered tremendous attention thanks to its various advantages such as flexibility [1], the large surface-to-volume ratio [2], and its functionalities such as energy harvesting [3], biomedical applications [4], and filtration systems [5]. Particularly, printing methods of nanofiber with a controllable manner using electrohydrodynamic phenomenon have been widely researched and developed to improve the performance of the devices [6, 7] and to expand the realm of the applications [8]. For example, the highly aligned piezoelectric nanofiber can generate high energy conversion efficiency. Also, the printed nanofiber in serpentine/helix

patterns enables piezoelectric nanogenerators to be highly flexible [9, 10]. Not only limited to energy-related applications, but various applications have also been developed and accomplished using nanofiber such as extracellular matrix scaffolds for tissue engineering [11], conducting electrodes [12], and photodetectors [13].

Electrospinning generates continuous nanofibers primarily by the electric force with the interplay between the physical, electrical, and rheological properties [14]. The electric field induces charges to the surface of the droplet, in which the mutual charges cause a repulsive force against the surface tension. As the electric field exceeds the critical point at which the repulsive force exceeds the surface tension, an ejection of charged jet occurs from the solution [15]. In electrospinning, there are several modes of jetting such as cone-jet, tilted-jet,

<sup>3</sup> Author to whom any correspondence should be addressed.

and multiple-jet, which are mainly dependent upon the balance between the electrostatic force and flow rate [14, 16]. Among those jetting modes, the cone-jet mode is considered the most stable method to generate a continuous nanofiber [17]. The cone-jet mode occurs when the normal electric stress and surface tension are balanced, at which the steady Taylor cone is formed [18].

Despite the stable and continuous nanofiber printing by the cone-jet mode, there is still room for the enhancement of nanofiber printing so that it can be integrated into microscale devices. The miniaturization of the coiling diameter (amplitude) is particularly desirable because the coiling diameter determines the resolution of patterns. Previously, a coiling diameter of 300  $\mu\text{m}$  using cone-jet mode was reported using polyethylene oxide (PEO) and polyvinylidene fluoride polymers [19, 20]. Recently, a reduced coiling diameter of 70  $\mu\text{m}$  was reported by utilizing both AC voltage of 300 V and DC voltage of 1.3 kV [21]. However, further reduction of the coiling diameter is required to curtail jet travel distance (JTD). A short JTD can minimize the jet buckling energy at the onset of contact with a collector so that the nanofiber is deposited with the smaller coiling diameter [22]. Reducing the JTD in the cone-jet mode is challenging because it leads to an electric spark due to the excessive electric field strength [23]. In addition, in the cone-jet mode, reducing the JTD can cause the presence of a great portion of the solvent in the jet upon deposition due to very short jet travel time that prevents solvent evaporation [24, 25]. Alternatively, increasing the collector velocity in the cone-jet mode can provide a pathway to reduce the coiling diameter of the nanofiber. A significant increment of the collector velocity from 60  $\text{mm s}^{-1}$  to 120  $\text{mm s}^{-1}$  was tested to change the coiling diameter from 300  $\mu\text{m}$  to 150  $\mu\text{m}$  [20]; however, the realization of sub-10  $\mu\text{m}$  coiling diameter has not been reported up until now, to the best of our knowledge.

Herein, we present droplet-jet mode near-field electrospinning (DJ-NFES) that can produce a precisely controlled helix nanofiber-pattern. In the droplet-jet mode, a microscale Taylor-cone is formed at the air-liquid interface of a droplet through an external stimulus. Through the microscale Taylor-cone, the jet can be developed to the nanoscale in a very short period of time, allowing further reduction of JTD. Thanks to the microscale JTD and Taylor-cone, nanofiber with a sub-10  $\mu\text{m}$  coiling diameter is successfully patterned. Also, it is found that the coiling diameter and the coiling frequency can be controlled by adjusting the droplet size in the droplet-jet mode. The DJ-NFES will be a new promising technique to generate controlled and continuous nanofiber with high-resolution, ultimately for the construction of microscale devices.

## 2. Methods

### 2.1. Experiment

To operate the droplet-jet mode, a vision-assisted printing system was built, as shown in figure 1(A). The system includes a  $xy$ -stage (Newport®, ONE-XY100),  $z$  stage (Newport®, GTS30V), voltage supply (Stanford Research System®, PS350), pneumatic pump (World Precision Instrument®,

PV820), and long-distance microscope (Infinity®, K2). All the listed devices were incorporated into the system by an in-house GUI (National Instrument®, LabVIEW) for reliable operation. In the droplet-jet mode, a jet flow rate is extremely low such that it is not even practically measurable. Therefore, the Vision-system using LabVIEW® was used to monitor and trace the droplet size in real-time. Then, the pneumatic pump can apply a pressure not only to maintain the same droplet size but also to change the droplet size. In this study, Polyethylene oxide (PEO; MW = 4000000  $\text{g mol}^{-1}$ ; Sigma Aldrich) was dissolved in deionized water to prepare the PEO polymer solution of 1.5% wt (surface tension  $\sim 55 \text{ mN m}^{-1}$ ), and then the polymer solution was loaded in a 5 ml syringe with a 32-gauge metal capillary (Nordson®).

The DJ-NFES utilizes a very low applied voltage between 300 and 1000 V, which enables to conserve the sphere-shape droplet. However, in this case, normal electric stress is too low to overcome the surface tension, thereby no ejection of the jet occurs. To resolve this issue, a mechanical drawing method should be performed to initiate the jet out of the meniscus [26–28]. Once the thin jet is mechanically drawn out of the droplet, the thin jet is exposed to a strong tangential electric force, creating shear stress on the jet which moves the jet in the direction of the electric field.

### 2.2. Characterization

**2.2.1. Droplet size control and measurement.** The droplet size during the droplet-jet mode was controlled and measured through real-time analysis of video images that were captured by the long-distance microscope as shown in figure 1(B). The circular peripheral shape of a droplet was automatically featured with the software and the corresponding droplet size (figure 1(B)) was calculated accordingly, reflecting changes of the value at any instance. The pneumatic pump was used to control the droplet size instead of the typical stepper-motor-based syringe pump. The pneumatic pump can provide holding pressure to prevent backfilling of the droplet caused by capillary force.

**2.2.2. Measurement using scanning electron microscopy (SEM).** A nanofiber from the droplet-jet mode was deposited on the silicon wafer in different pattern-types, as shown in figure 1(C). In order to measure and obtain the fiber diameter and the cross-section image, we used scanning electron microscopy (SEM, FEI Helios Nanolab 650). Prior to the measurements, the sample was coated with an approximately 10 nm layer of titanium to prevent the charging effect during SEM operation [29]. For the cross-section measurement, the deposited nanofiber on the wafer was dipped into liquid nitrogen in order to prevent potential damage to the nanofiber [30].

## 3. Results and discussion

### 3.1. Cone-jet mode and droplet-jet mode

To compare the droplet-jet mode with the cone-jet mode at a short JTD, the transition from the cone-jet to the droplet-jet

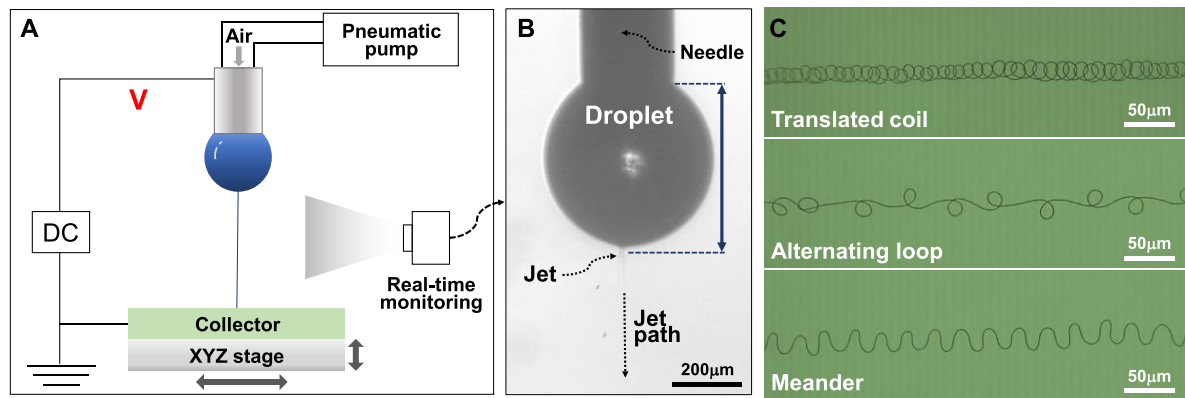


**Figure 1.** (A) Experimental setup of NFES including voltage supply, pneumatic pump,  $xy$  stage,  $z$  stage, and real-time monitoring system to study the effect of droplet size. (B) Actual image of droplet-jet captured by the long-distance microscope during NFES operation. (C) Optical image of the patterned nanofibers in different shapes including translated coil, alternating loop, and meanders.

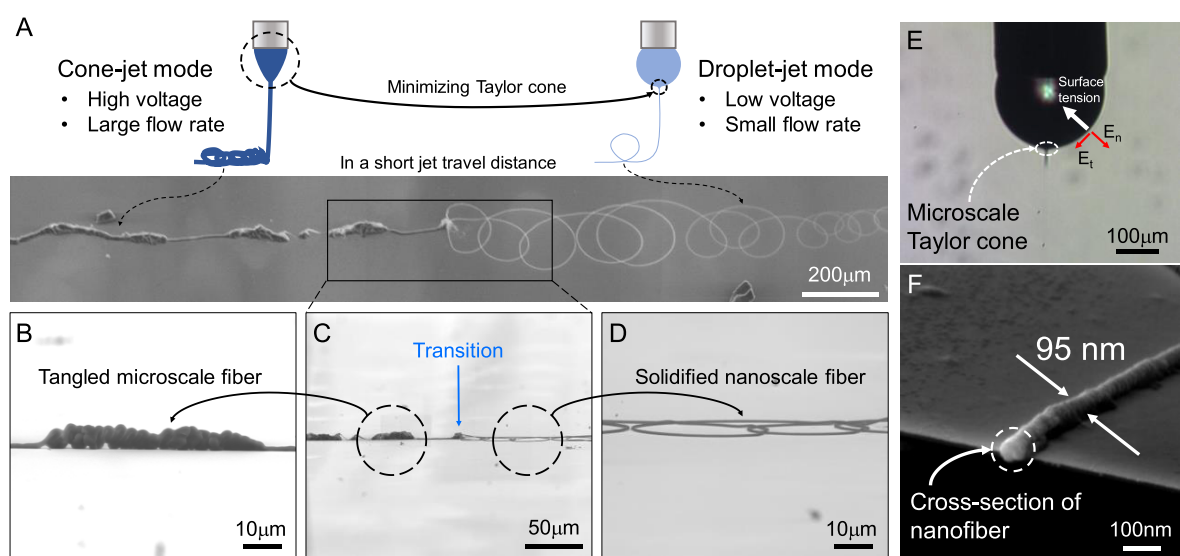


**Figure 2.** (A) SEM image showing a conformational change of the fiber patterns with respect to jet condition transition from cone-jet mode (left) to droplet-jet mode (right) at the tip-to-collector distance (TTCD) of 1 mm. (B) Thick and tangled fiber from the cone-jet mode. (C) Transition section from the cone-jet mode to the droplet-jet mode. (D) Solidified nanoscale fiber from the droplet-jet mode. (E) Optical image showing the ejection point and jet path of the droplet-jet mode. (F) SEM image showing the cylindrical cross-section of deposited nanofiber from the cone-jet.

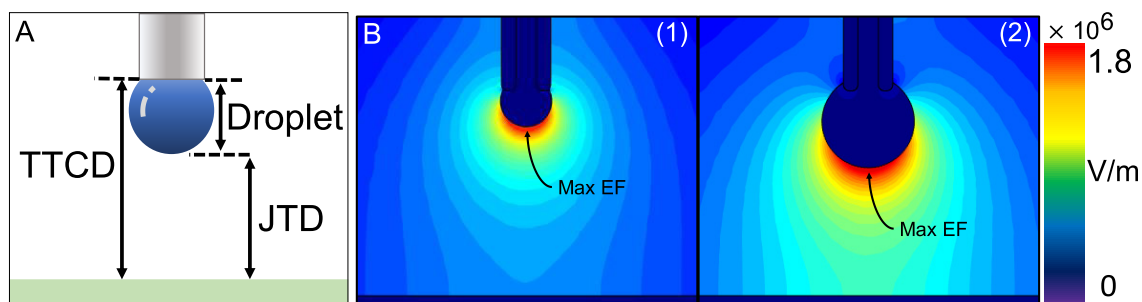


**Figure 3.** (A) Configuration of droplet-jet mode including TTCD, droplet, and JTD. (B) Electric field strength distribution at the droplet size of 0.2 and 0.4 mm for (1) and (2), respectively.

was continuously performed by continuously reducing the applied voltage. As shown in figures 2(A)–(D), the cone-jet mode produced a tangled fiber with microscale diameter ( $\sim 7 \mu\text{m}$ ) whereas the droplet-jet mode generated a nanofiber. In the cone-jet mode, the jet was attenuated to a thin jet through the Taylor-cone; the minimum distance based on

the geometry of the cone was required to acquire the thin jet. Thus, when a short JTD was used in the cone-jet mode, a bundled, thick and viscous microscale fiber was deposited as both the actual JTD and time were not sufficient to fully evaporate the solvent and to form nanoscale jet (figure 2(B)). On the other hand, the droplet-jet mode ejected a

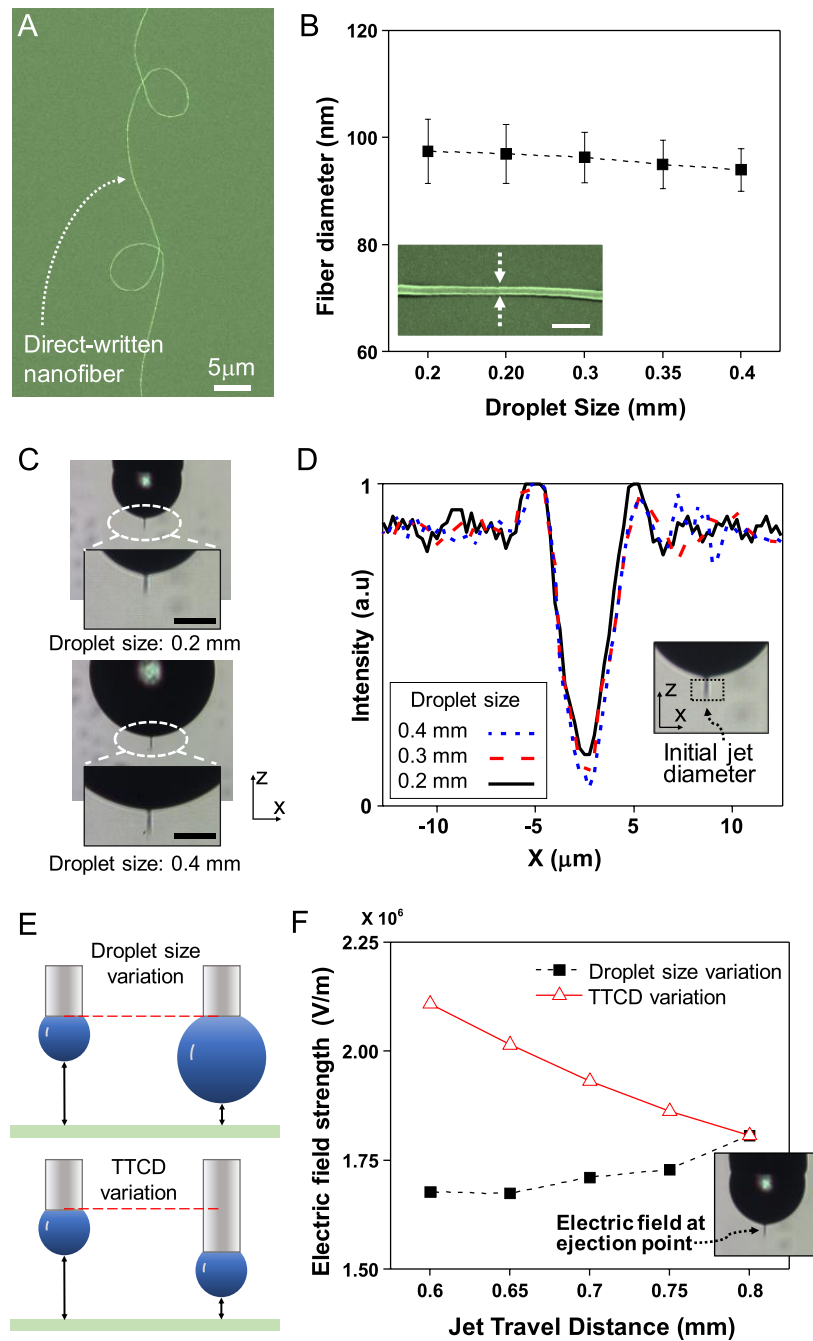


**Figure 4.** (A) SEM image of printed nanofiber. (B) Fiber diameter as a function of droplet size (scale bar: 200 nm). (C) Angular frequency as a function of droplet size (scale bar: 100  $\mu\text{m}$ ). (D) Optical images of the jet diameter of droplet size of 0.2 and 0.4 mm at the ejection point. (E) Comparison between the droplet size variation and the TTCD variation for the same JTD. (F) The difference of the trend on the electric field strength at the ejection point between the droplet size and the TTCD variation.

much thinner jet out of the droplet by forming a micro-scale Taylor-cone at the air-liquid interface of a droplet as shown in figure 2(E). Such a small Taylor cone leads to the formation of the nanoscale jet in very short period time, and thus, the initial jet diameter from the droplet-jet mode is much smaller than the jet from the cone-jet mode. A greater electric force exerts on the jet as the jet becomes thinner [30]. Hence, the thin jet from the droplet-jet mode experiences a stronger electric force, enhancing the electrical stretching on the jet and evaporation of the solvent. As a result, the droplet-jet mode enables the generation of a nanofiber with the cylindrical cross-section as identified by SEM in figures 2(D) and (F).

Typically, flat-ribbon shape or beads were identified when the jet was deposited on the collector with the presence of the solvent [31]. Hence, the cylindrical cross-section of the deposited nanofiber suggests that most of the solvent already evaporated before deposition. If the collector is moving faster than the jet impact velocity, then the jet is dragged to the collector moving direction (supplementary information available online, figure S1, [stacks.iop.org/JMM/29/045004/mmedia](https://stacks.iop.org/JMM/29/045004/mmedia)). Therefore, the collector velocity should be set either equal to or less than the jet impact velocity. In this case, the jet is primarily driven by the tangential electric force, thereby remaining at the apex of the droplet.



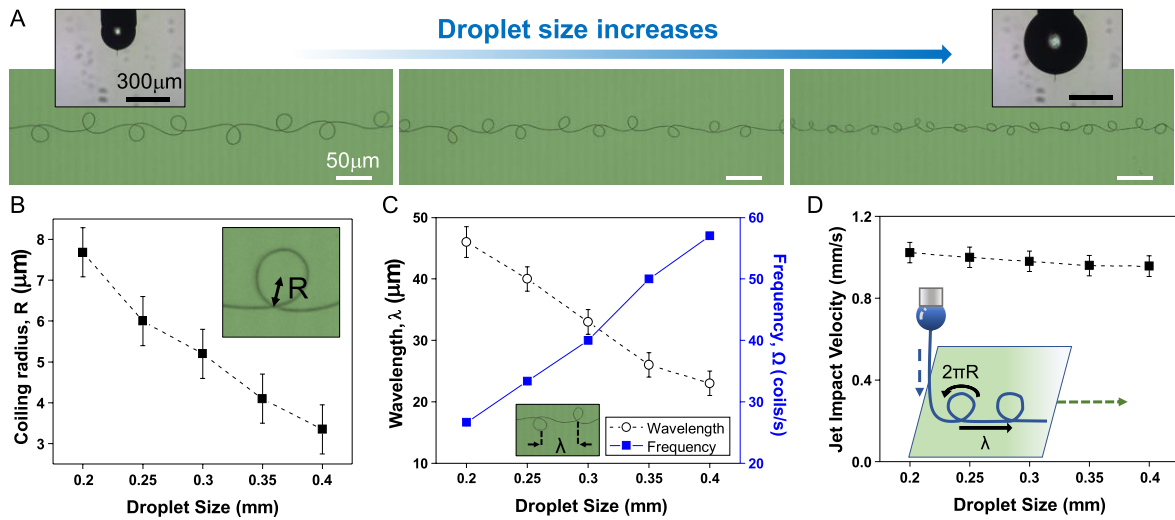


**Figure 5.** (A) Deposition manner change under varying the droplet size from 0.2 to 0.4 mm. (B) Coiling radius of nanofiber pattern as a function of droplet size. (C) The wavelength of the nanofiber pattern as a function of droplet size. (D) Jet impact velocity as a function of droplet size.

### 3.2. The effect of droplet size in droplet-jet mode

**3.2.1. Configuration of droplet-jet mode.** As a JTD is less than 500 μm in the droplet-jet mode, droplet size in addition to existing process parameters comes to play a role since droplet size takes up a big portion of the tip-to-collector distance (TTCD) as shown in figure 3(A). Therefore, the size of the droplet has a strong influence on the electric field distribution and the JTD. To study the influence of the droplet size variation, DJ-NFES was performed where only the droplet size varied from 0.2 to 0.4 mm whereas other major parameters such as the applied voltage and the TTCD were fixed at 600 V and 1 mm, respectively. If the size of the droplet is too small or too big, the DJ-NFES process can be interrupted by an excessive or inadequate electric force in the droplet-jet region, resulting in multi-jetting or discontinuity of jet. The electric field simulation from COMSOL® shows that the general electric field strength distribution was changed when the droplet size increased from 0.2 to 0.4 mm as shown in figures 3(B) (1) and (2). Despite the modification of the electric field distribution, the electric field around the droplet remains similar, with a maximum strength of  $1.8 \times 10^6 \text{ V m}^{-1}$  for a droplet size of both 0.2 and 0.4 mm. As a result, this consistent electric field strength around the droplet throughout the changing droplet size maintains the droplet's spherical shape that is dominated by the surface tension. Therefore, the droplet-jet mode can be preserved throughout changing droplet size (supplementary information available, figure S2). The ejection of the jet occurs at the maximum electric field strength, and the maximum electric field strength is found at the apex of the droplet as long as the symmetry of the droplet is conserved as shown in figures 3(B)(1) and (2).

**3.2.2. Influence on fiber diameter.** To understand how the variation of the droplet size affects the fiber diameter, SEM was used to measure the diameter of the direct-written fiber as shown in figure 4(A). Figure 4(B) shows the measured fiber diameter as the droplet size changes from 0.2 to 0.4 mm.

**Table 1.** Experimental parameters.

Parameters	Symbol	Value
Average fiber diameter [nm]	$R$	95
Solution density [ $\text{kg m}^{-3}$ ]	$\rho$	$0.99 \times 10^3$
Conductivity of PEO solution [ $\text{mS m}^{-1}$ ]	$\sigma$	8.49
Permittivity of free space [ $\text{F m}^{-1}$ ]	$\epsilon_0$	$8.854 \times 10^{-12}$
Gravitational acceleration [ $\text{m s}^{-2}$ ]	$g$	9.8
Average electric field strength [ $\text{V m}^{-1}$ ]	$E$	$1.2 \times 10^6$

No significant change of the fiber diameter was observed, although the trend showed a very slight decrease from 98 to 94 nm. Nonetheless, the variation of fiber diameter under a varying droplet size is negligibly small. To compare the initial fiber diameter at the ejection point of each droplet with the final one, the optical images were captured by the long-distance camera during the droplet-jet mode as shown in figure 4(C). Then, the image was processed to estimate the physical dimension of the jet by constructing the intensity plot of the jet ejection region (supplementary information available, S3). From the image analysis, for the droplet size from 0.2 to 0.4 mm, fiber diameter at the ejection point is almost identical to the final diameter as shown in figure 4(D).

As visualized in figure 4(E), the JTD can be controlled by either the TTCD or the droplet size. The JTD is changed as the droplet size varies with the fixed TTCD (figure 4(E)-top). Also, the JTD is changed as the TTCD varies with the fixed droplet size (figure 4(E)-bottom). In some literature, an increase in the fiber diameter was reported as the JTD decreased [27, 31]. However, the variation of the droplet size does not have a significant effect on the fiber diameter based on our observation. Thus, it is worth investigating why the fiber diameter did not increase as the JTD decreased by increasing the droplet size. It is noted that the change of droplet size has a relatively different degree of influence on the electric field strength, depending on TTCD. Figure 4(F) shows the different trend of the electric field strength change at the ejection point when the variation

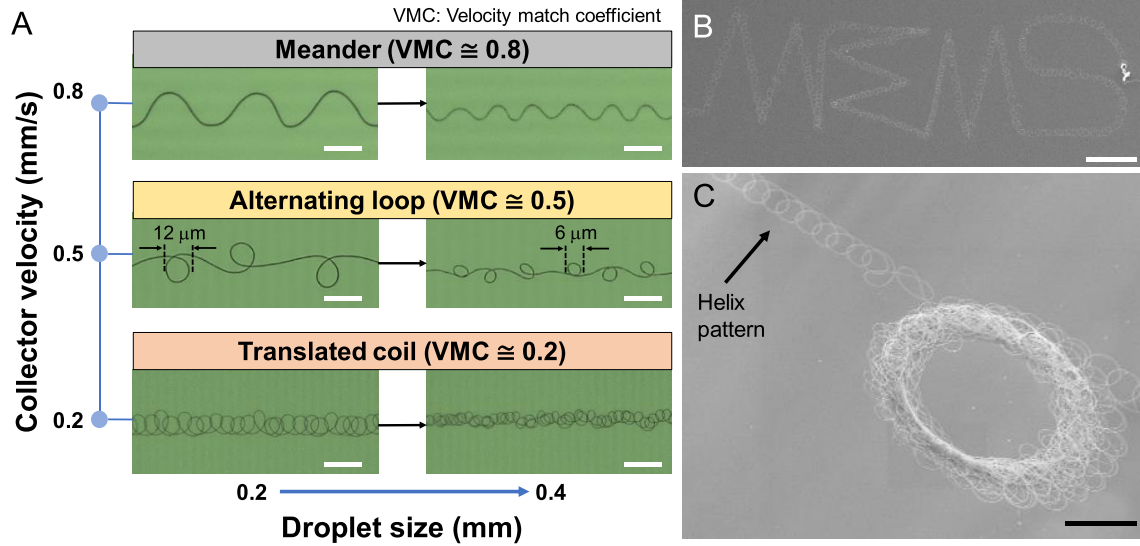


**Figure 6.** (A) Change in amplitude and wavelength of nanofiber pattern with varying droplet size (scale bar: 10 μm). (B) SEM image of direct-written 'MEMS' letters in 100 × 400 μm made by nanofiber with the coiling diameter of sub-10 μm (scale bar: 50 μm). (C) SEM image of the direct-written pore with the diameter of 100 μm by the nanofiber coils with the 25 μm diameter (scale bar: 50 μm).

of TTCD and the droplet size were applied. While the change of droplet size (solid black square) only varies the electric field strength by 7% (decrement), the change of TTCD (blank red triangle) varies the electric field strength by 15% (increment). This result indicates that the diameter of the jet at the onset of initiation is conserved when the droplet size varies.

**3.2.3. Influence on nanofiber pattern.** While varying the droplet size, different deposition conditions in terms of the coiling diameter ( $R$ ), wavelength ( $\lambda$ ), and coiling frequency ( $\Omega$ ) were found as shown in figure 5(A). As the droplet size increased, reductions of both the coiling radius and the wavelength were observed whereas the coiling frequency increased as shown in figures 5(B) and (C). In order to uncover how those modifications of the patterns affect the jet impact velocity ( $V_{\text{fiber}}$ ), the jet impact velocity was estimated by  $V_f = (2\pi R + \lambda)/T$  as presented in figure 5(D). Although the coiling radius and the wavelength change significantly, the actual jet impact velocity shows no significant changes and show a steady response. It is because the normalized coiling radius increases at the same rate as the frequency decreases, resulting in almost no change of the jet impact velocity (supplementary information, S4). This result implies that the coiling radius and the frequency vary at the same rate to balance out the jet impact velocity when the droplet size changes. To understand why these changes are caused by the variation of the droplet size, the equation to express the coiling radius in electrospinning needs to be examined. By taking account of the experimental parameters in table 1, the scaled gravity force per unit length ( $F_g \sim \rho g r^2$ ) and the scaled inertia force per unit length ( $F_i \sim \rho r^2 \Omega^2 R$ ) are found to be negligible, compared to the scaled electrostatic force per unit length ( $F_e \sim \varepsilon_0 r E^2$ ) [32], where  $\varepsilon_0$  is the permittivity of free space,  $g$  is the gravitational acceleration,  $\rho$  is the density of the solution,  $r$  is the diameter of the fiber, and  $E$  is the electric field strength [33]. Then, a balance between the electrostatic torque

( $\sim F_e R^2$ ) and the elastic torque ( $\sim YI/R$ ) determine the coiling radius [32]. The coiling radius ( $R$ ) is then expressed as,

$$R \sim d^{\frac{2}{3}} \left( \frac{Yr^3}{\varepsilon_0 V^2} \right)^{\frac{1}{3}} \quad (1)$$

where  $Y$  is Young's modulus of fiber,  $I$  is the area moment of inertia ( $\sim r^4$ ),  $V$  is the applied voltage, and  $d$  is the distance of separation between the positive and the negative charges, which is from the air-liquid interface of the droplet to the collector ( $\cong \text{JTD}$ ).

Equation (1) states that a decrease of the distance results in a reduction of the coiling radius when all other parameters are constant. In this equation, Young's modulus and the permittivity of free space can be assumed as a constant. From the test results discussed above, the measured diameter ( $r$ ) shows almost no variation (figure 4(B)) and the applied voltage ( $V$ ) is fixed. Therefore, the increasing droplet size curtails the distance ( $d$ ), which leads to the reduction in the coiling radius ( $R$ ). Accordingly, the coiling frequency should increase as the jet impact velocity is constant (figure 5(C)). Thus, it is concluded that the droplet size variation can maintain the jet impact velocity while modifying the coiling radius and the wavelength of the pattern.

**3.2.4. Control of helix nanofiber pattern within the same type of pattern.** When the jet was deposited on the moving collector at the higher rate than the rate at which the jet forms in a straight line, the jet was deposited as different forms such as translated coil, alternating loop, and meander. Each pattern type was determined by the velocity match coefficient ( $V_{\text{collector}}/V_{\text{fiber}}$ ), where the  $V_{\text{collector}}$  is the collector velocity and  $V_{\text{fiber}}$  is the jet impact velocity [20, 34]. Since the jet impact velocity does not change as the droplet size varies (figure 5(D)), the velocity match coefficient should be maintained as long as the collector velocity is constant. To validate this, three different types of patterns were obtained by matching

the velocity match coefficient as shown in figure 6(A). As a result of the changing droplet size, the same type of pattern was continued while the coiling radius (amplitude), the wavelength, and the frequency were changed as presented in figure 6(A). In any pattern type, the same trend of change is observed, where the coiling radius decreases and the frequency increases. Therefore, the droplet size variation was utilized to change the coiling radius (amplitude) and the frequency within the same pattern type.

By controlling the droplet size and the JTD, the four letter words 'MEMS' in  $100 \times 400 \mu\text{m}$  was direct-written in the shape of the translated coil with the coiling diameter of sub- $10 \mu\text{m}$  as shown in figure 6(B). The direct-written coil pattern of nanofiber using the droplet-jet mode can be stacked up to make a porous nanofiber in microscale as shown in figure 6(C).

#### 4. Conclusion

In this paper, DJ-NFES was studied for precisely controlled helix patterns of nanofiber. The droplet-jet mode was demonstrated to generate solidified nanofiber with a much shorter JTD compared to the cone-jet mode. The JTD determines the size of the coiling diameter; thus, the droplet-jet mode can greatly reduce the coiling diameter to less than sub- $10 \mu\text{m}$ . The droplet size in the droplet-jet mode plays a role as one of the process parameters. The fiber diameter and the jet impact velocity showed very little variation when changing the droplet size. Because of the negligible change in the diameter and the jet impact velocity, variation of the droplet size enables control of the coiling diameter and the frequency within the same type of pattern. Using the droplet-jet mode, the nanofiber with a coiling diameter of less than sub- $10 \mu\text{m}$  can be direct-written in micro-scale resolution. This direct-written nanofiber for controlled helix pattern in micro-scale can be used for fiber-based applications including flexible electronics and scaffolds for tissue engineering.

#### Acknowledgments

This work made use of the University of Utah USTAR shared facilities supported, in part, by the MRSEC Program of the NSF under Award No. DMR-1121252. This work was supported by the KIST Institutional Program (Project Nos. 2E29700 and 2E29710).

#### ORCID iDs

Dongwoon Shin  <https://orcid.org/0000-0002-4545-4802>

#### References

- [1] Wu H *et al* 2011 Low reflectivity and high flexibility of tin-doped indium oxide nanofiber transparent electrodes *J. Am. Chem. Soc.* **133** 27–9
- [2] Zheng G, Yang Y, Cha J J, Hong S S and Cui Y 2011 Hollow carbon nanofiber-encapsulated sulfur cathodes for high specific capacity rechargeable lithium batteries *Nano Lett.* **11** 4462–7
- [3] Chang C, Tran V H, Wang J and Fuh Y-K 2010 Direct-write piezoelectric polymeric nanogenerator with high energy conversion efficiency *Nano Lett.* **10** 726–31
- [4] Yoshimoto H, Shin Y M, Terai H and Vacanti J P 2003 A biodegradable nanofiber scaffold by electrospinning and its potential for bone tissue engineering *Biomaterials* **24** 2077–82
- [5] Qin X-H and Wang S-Y 2006 Filtration properties of electrospinning nanofibers *J. Appl. Polym. Sci.* **102** 1285–90
- [6] Ye D, Ding Y, Duan Y, Su J, Yin Z and Huang Y A 2018 Large-scale direct-writing of aligned nanofibers for flexible electronics *Small* **14** 1703521
- [7] Teo W E and Ramakrishna S 2006 A review on electrospinning design and nanofibre assemblies *Nanotechnology* **17** R89–106
- [8] Onses M S, Sutanto E, Ferreira P M, Alleyne A G and Rogers J A 2015 Mechanisms, capabilities, and applications of high-resolution electrohydrodynamic jet printing *Small* **11** 4237–66
- [9] Duan Y *et al* 2017 Ultra-stretchable piezoelectric nanogenerators via large-scale aligned fractal inspired micro/nanofibers *Polymers* **9** 714
- [10] Chang J, Dommer M, Chang C and Lin L 2012 Piezoelectric nanofibers for energy scavenging applications *Nano Energy* **1** 356–71
- [11] He J, Xia P and Li D 2016 Development of melt electrohydrodynamic 3D printing for complex microscale poly ( $\epsilon$ -caprolactone) scaffolds *Biofabrication* **8** 035008
- [12] Lee Y, Kim T-S, Min S-Y, Xu W, Jeong S-H, Seo H-K and Lee T-W 2014 Individually position-addressable metal-nanofiber electrodes for large-area electronics *Adv. Mater.* **26** 8010–6
- [13] Liu X, Gu L, Zhang Q, Wu J, Long Y and Fan Z 2014 All-printable band-edge modulated ZnO nanowire photodetectors with ultra-high detectivity *Nat. Commun.* **5** 4007
- [14] Lee A, Jin H, Dang H-W, Choi K-H and Ahn K H 2013 Optimization of experimental parameters to determine the jetting regimes in electrohydrodynamic printing *Langmuir* **29** 13630–9
- [15] Taylor G 1969 Electrically driven jets *Proc. R. Soc. A* **313** 453–75
- [16] Yu M, Ahn K H and Lee S J 2016 Design optimization of ink in electrohydrodynamic jet printing: effect of viscoelasticity on the formation of Taylor cone jet *Mater. Des.* **89** 109–15
- [17] Collins R T, Harris M T and Basaran O A 2007 Breakup of electrified jets *J. Fluid Mech.* **588** 75–129
- [18] Yarin A L, Koombhongse S and Reneker D H 2001 Taylor cone and jetting from liquid droplets in electrospinning of nanofibers *J. Appl. Phys.* **90** 2201–21
- [19] Xin Y and Reneker D H 2012 Hierarchical polystyrene patterns produced by electrospinning *Polymer* **53** 4254–61
- [20] Duan Y, Ding Y, Xu Z, Huang Y and Yin Z 2017 Helix electrohydrodynamic printing of highly aligned serpentine micro/nanofibers *Polymers* **9** 434
- [21] Fang F *et al* 2015 Controllable direct-writing of serpentine micro/nano structures via low voltage electrospinning *Polymers* **7** 1577–86
- [22] Morris S W, Dawes J H P, Ribe N M and Lister J R 2008 Meandering instability of a viscous thread *Phys. Rev. E* **77** 066218
- [23] Zhang D, Karki A B, Rutman D, Young D P, Wang A, Cocke D, Ho T H and Guo Z 2009 Electrospun polyacrylonitrile nanocomposite fibers reinforced with



- Fe<sub>3</sub>O<sub>4</sub> nanoparticles: fabrication and property analysis *Polymer* **50** 4189–98
- [24] Tripatanasuwan S, Zhong Z and Reneker D H 2007 Effect of evaporation and solidification of the charged jet in electrospinning of poly(ethylene oxide) aqueous solution *Polymer* **48** 5742–6
- [25] Wei C, Dong J and Fitts E P 2013 Direct fabrication of high-resolution three-dimensional polymeric scaffolds using electrohydrodynamic hot jet plotting *J. Micromech. Microeng* **23** 25017–9
- [26] Shin D, Kim J and Chang J 2018 Experimental study on jet impact speed in near-field electrospinning for precise patterning of nanofiber *J. Manuf. Process.* **36** 231–7
- [27] Chang C, Limkrailassiri K and Lin L 2008 Continuous near-field electrospinning for large area deposition of orderly nanofiber patterns *Appl. Phys. Lett.* **93** 123111
- [28] Lei T P, Lu X Z and Yang F 2015 Fabrication of various micro/nano structures by modified near-field electrospinning *AIP Adv.* **5** 041301
- [29] Kim K H, Akase Z, Suzuki T and Shindo D 2010 Charging effects on SEM/SIM contrast of metal/insulator system in various metallic coating conditions *Mater. Trans.* **51** 1080–3
- [30] Kim J, Shin D, Han K-B and Chang J 2018 A quantification of jet speed and nanofiber deposition rate in near-field electrospinning through novel image processing *J. Micro Nanomanuf.* **6** 031002
- [31] Zhou F-L, Hubbard P L, Eichhorn S J and Parker G J M 2011 Jet deposition in near-field electrospinning of patterned polycaprolactone and sugar-polycaprolactone core-shell fibres *Polymer* **52** 3603–10
- [32] Kim H-Y, Lee M, Park K J, Kim S and Mahadevan L 2010 Nanopottery: coiling of electrospun polymer nanofibers *Nano Lett* **10** 2138–40
- [33] Kong T, Li J, Liu Z, Zhou Z, Hon P, Ng Y, Wang L and Shum H C 2015 Rapid mixing of viscous liquids by electrical coiling *Sci. Rep.* **6** 19606
- [34] Brun P-T, Audoly B, Ribe N M, Eaves T S and Lister J R 2015 Liquid ropes: a geometrical model for thin viscous jet instabilities *Phys. Rev. Lett.* **114** 174501